2020 IEEE/RSJ International Conference on Intelligent Robots and Systems (IROS)
October 25-29, 2020, Las Vegas, NV, USA (Virtual)

Design, Analysis and Preliminary Validation of a 3-DOF Rotational Inertia Generator*

Jean-Félix Tremblay-Bugeaud[1], Thierry Laliberté[1] and Clément Gosselin[1]

***Abstract*— This paper investigates the design of a three-degree-of-freedom rotational inertia generator using the gyroscopic effect to provide ungrounded torque feedback. It uses a rotating mass in order to influence the torques needed to move the device, creating a perceived inertia. The dynamic model and the control law of the device are derived, along with those of a comparable concept using three flywheels instead of a gyroscope. Both models are then validated through simulations. Further simulations are conducted to establish motor torque and velocity requirements, and the gyroscopic concept is identified as having the less demanding requirements. The mechatronic design of a prototype of an inertia generator is presented, along with modifications to the dynamic model. Preliminary experimental validations are conducted. As the prototype faces instability issues when using the flywheels at high velocities, they are conducted using 0 RPM initial velocities. The results confirm that it is possible to both reduce and increase the rendered inertia even with current limitations. Finally, improvements for a second version of the prototype are discussed.**

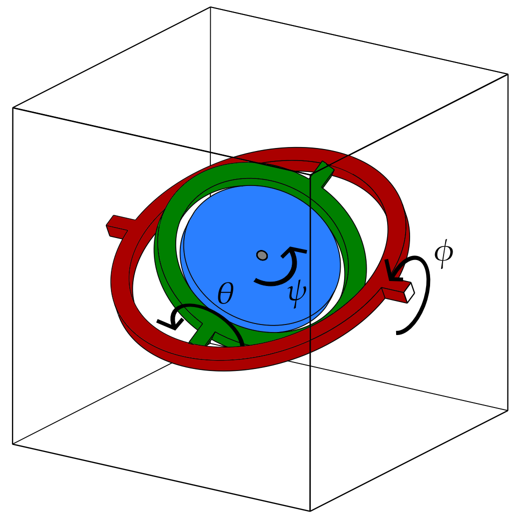

Fig. 1: General layout for an inertia generator using a double gimbal gyroscope (DGG).

I. Introduction

Haptic devices are a great tool to enhance the experience of a user. They can aid the user to navigate and reach a designated location, as demonstrated by the research on haptic compasses [1]-[3]. They also allow interactions with a virtual environment [4][5], providing a more immersive experience [6]. These types of devices are usually designed as hand-held apparatuses which means that they require the ability to provide a force feedback without being grounded. Some, like the iTorqU [7], are based on the gyroscopic effect to achieve this while others, like the TorqueBAR [8], even use gravity through the displacement of the centre of mass.

The aim of this paper is to create a hand-held haptic interface with programmable rotational inertia using an ungrounded torque feedback method based on the gyroscopic effect. This type of device, also called inertia generator, is capable of inducing torques to a user typically by displacing a mass within a frame. By exploiting the reaction forces between these bodies, it is possible to either aid or hinder a user in moving the frame, thereby simulating a prescribed inertia. This inertia generator provides a new way of approaching interactions with a user, since it doesn't use preprogrammed torque profiles to represent an action between two objects, or an object and the environment. Instead, it is controlled reactively through the prescribed inertia, and lets the user feel a single object by itself. This type of feature could be implemented to further increase immersion in VR applications. It could also serve as a physical readaptation tool, whereby it could incrementally monitor the muscular force capabilities of a person while providing force and torque data. In previous work, a one-degree-of-freedom (1-DOF) prototype for translational inertia was developed [9]. Here, a 3-DOF rotational inertia generator is investigated. This hand-held device will be capable of rendering a prescribed perceived moment of inertia when manipulated.

Firstly, the dynamic modelling of the 3-DOF concept using the gyroscopic effect is presented. Then, a second concept directly exploiting motor reaction forces is established as a basis of comparison. Both concepts are simulated using a mathematical model, and they are compared in terms of torque and velocity requirements. The physical prototype is then described, with preliminary experiments presented to validate the developed dynamic model. Lastly, improvements for future work are discussed.

II. Dynamic Modelling of a 3-DOF Inertia Generator

A. Double Gimbal Gyroscope Concept

The double gimbal gyroscope (DGG) concept can be treated as a serial spherical rotational mechanism, with

*The authors would like to acknowledge the financial support of the Natural Sciences and Engineering Research Council of Canada (NSERC) and of the Canada Research Chair Program.

[1]Jean-Félix Tremblay-Bugeaud, Thierry Laliberté and Clément Gosselin are with the Department of Mechanical Engineering, Université Laval, 1065 Avenue de la médecine, Québec, QC, Canada
jean-felix.tremblay-bugeaud.1@ulaval.ca
Thierry.Laliberte@gmc.ulaval.ca
Clement.Gosselin@gmc.ulaval.ca

978-1-7281-6211-9/20/$31.00 ©2020 IEEE

each of the links having their centre of mass at the centre of rotation of the device, as illustrated in Figure 1. The XYZ-Euler convention is used to describe the orientation of the flywheel (end-link) of the gyroscope with respect to the frame of the device, while only the angular velocities are used to describe the motion of the frame of the device with respect to a fixed frame. This means that the frame uses only angular velocities expressed in a non-inertial frame, while the gyroscope uses the coordinates ϕ, θ, ψ (joint coordinates, which also correspond to the Euler angles) for its respective XYZ coordinates. Angular velocities of the different bodies are given by

$$\begin{aligned}
[\vec{\omega}_f]_B &= [\omega_x,\ \omega_y,\ \omega_z]^{\mathrm{T}} \\
[\vec{\omega}_{g1}]_1 &= \dot{\phi}\vec{e}_1 + [\vec{\omega}_f]_1 \\
[\vec{\omega}_{g2}]_2 &= \dot{\theta}\vec{e}_2 + [\vec{\omega}_{g1}]_2 \\
[\vec{\omega}_w]_2 &= \dot{\psi}\vec{e}_3 + [\vec{\omega}_{g2}]_2 \,,
\end{aligned}$$

where subscripts f, $g1$, $g2$ and w represent the frame, the first and second gimbal, and the flywheel respectively, whereas subscripts B, 1, and 2 mean that the corresponding vectors are expressed in the body, first gimbal, or second gimbal reference frames. Vectors $\vec{e}_1$, $\vec{e}_2$, and $\vec{e}_3$ represent unit vectors along the X, Y and Z-axes of the frame of reference in which they are used. Furthermore, coordinate changes are given by

$$\begin{aligned}
[\vec{\omega}_f]_1 &= \mathbf{R}_x^{\mathrm{T}}(\phi)\,[\vec{\omega}_f]_B \\
[\vec{\omega}_{g1}]_2 &= \mathbf{R}_y^{\mathrm{T}}(\theta)\,[\vec{\omega}_{g1}]_1 \,,
\end{aligned}$$

where $\mathbf{R}_x(\phi)$ and $\mathbf{R}_y(\theta)$ are the X and Y rotation matrices according to the Euler convention. For each of the bodies, assuming a concentric configuration, i.e., assuming that all bodies have their centre of mass at the centre of rotation, the kinetic energy is given by

$$\begin{aligned}
T_f &= \frac{1}{2}\,[\vec{\omega}_f]_B^{\mathrm{T}}\,[\mathbf{I}_f]_B\,[\vec{\omega}_f]_B \\
T_{g1} &= \frac{1}{2}\,[\vec{\omega}_{g1}]_1^{\mathrm{T}}\,[\mathbf{I}_{g1}]_1\,[\vec{\omega}_{g1}]_1 \\
T_{g2} &= \frac{1}{2}\,[\vec{\omega}_{g2}]_2^{\mathrm{T}}\,[\mathbf{I}_{g2}]_2\,[\vec{\omega}_{g2}]_2 \\
T_w &= \frac{1}{2}\,[\vec{\omega}_w]_2^{\mathrm{T}}\,[\mathbf{I}_w]_2\,[\vec{\omega}_w]_2 \,,
\end{aligned}$$

where $\mathbf{I}_i$ denotes de inertia matrix of body i, and with total kinetic energy given by

$$T = \sum_i T_i. \tag{1}$$

Assuming that the total kinetic energy can be expressed in terms of a generalized inertia matrix $\mathbf{M}$ such that

$$T = \frac{1}{2}\dot{\vec{\Theta}}^{\mathrm{T}}\mathbf{M}\dot{\vec{\Theta}}, \tag{2}$$

where $\dot{\vec{\Theta}} = \left[\omega_x,\ \omega_y,\ \omega_z,\ \dot{\phi},\ \dot{\theta},\ \dot{\psi}\right]^{\mathrm{T}}$, then $\mathbf{M} = \dfrac{\partial^2 T}{\partial \dot{\vec{\Theta}}^2}$ and the Lagrangian equations yield

$$\vec{\tau} - \vec{\Phi} = \frac{\mathrm{d}}{\mathrm{dt}}\frac{\partial \mathcal{L}}{\partial \dot{\vec{\Theta}}} - \frac{\partial \mathcal{L}}{\partial \vec{\Theta}} = \frac{\mathrm{d}}{\mathrm{dt}}\left[\mathbf{M}\dot{\vec{\Theta}}\right] - \frac{\partial T}{\partial \vec{\Theta}}, \tag{3}$$

where $\mathcal{L} = T - V$ and the potential energy V is constant since the centre of mass remains fixed. $\vec{\tau}$ is the vector of actuator torques, and $\vec{\Phi}$ contains the friction forces. By partitioning (3) into two sets of three equations, one for the frame and one for the gyroscope, (3) can be written as

$$\begin{bmatrix} \vec{\tau_a} - \vec{\Phi}_a \\ \vec{\tau_m} - \vec{\Phi}_m \end{bmatrix} = \frac{\mathrm{d}}{\mathrm{dt}}\left[\begin{bmatrix} \mathbf{M}_{11} & \mathbf{M}_{12} \\ \mathbf{M}_{21} & \mathbf{M}_{22} \end{bmatrix}\begin{bmatrix} \dot{\vec{\Theta}}_a \\ \dot{\vec{\Theta}}_m \end{bmatrix}\right] - \begin{bmatrix} \dfrac{\partial T}{\partial \vec{\Theta}_a} \\ \dfrac{\partial T}{\partial \vec{\Theta}_m} \end{bmatrix}, \tag{4}$$

where $\dot{\vec{\Theta}}_a = [\vec{\omega}_f]_B$, and $\vec{\Theta}_m = [\phi,\ \theta,\ \psi]^{\mathrm{T}}$. This means that $\vec{\Theta}_a$ is not an actual physical quantity since an angular velocity vector cannot be integrated, but this can be resolved by noting that the kinetic energy of the device is independent from the absolute orientation of the hand-held frame, meaning that $\frac{\partial T}{\partial \vec{\Theta}_a} = 0_{3\times 1}$. Also, $\vec{\Phi}_a = 0_{3\times 1}$ because the frame is manipulated by a user.

Since (4) is not taken from an inertial frame of reference, the first row gives

$$\begin{aligned}
\vec{\tau_a} &= \begin{bmatrix} \mathbf{M}_{11} & \mathbf{M}_{12} \end{bmatrix}\begin{bmatrix} \ddot{\vec{\Theta}}_a \\ \ddot{\vec{\Theta}}_m \end{bmatrix} + \vec{\Omega} \times \left[\begin{bmatrix} \mathbf{M}_{11} & \mathbf{M}_{12} \end{bmatrix}\dot{\vec{\Theta}}\right] \\
&\quad + \begin{bmatrix} \dot{\mathbf{M}}_{11} & \dot{\mathbf{M}}_{12} \end{bmatrix}\dot{\vec{\Theta}},
\end{aligned} \tag{5}$$

where $\vec{\Omega} = [\vec{\omega}_f]_B$. This is akin to the Newtonian equations of motion, and is a necessary way to build the equations in order to directly use a 3-axis gyroscope to measure the body motion of the device. The second row of (4) yields

$$\begin{aligned}
\vec{\tau_m} - \vec{\Phi}_m &= \begin{bmatrix} \mathbf{M}_{21} & \mathbf{M}_{22} \end{bmatrix}\ddot{\vec{\Theta}} \\
&\quad + \begin{bmatrix} \dot{\mathbf{M}}_{21} & \dot{\mathbf{M}}_{22} \end{bmatrix}\dot{\vec{\Theta}} - \frac{\partial T}{\partial \vec{\Theta}_m}.
\end{aligned} \tag{6}$$

To obtain the inertia generator effect, i.e., to render a desired inertia to the user, the torques appearing in (5) need to be equivalent to the torques needed to rotate an object of prescribed inertia $\mathbf{I}_a$, meaning

$$\begin{aligned}
T_a &= \frac{1}{2}\,[\vec{\omega}_f]_B^T\,[\mathbf{I}_a]_B\,[\vec{\omega}_f]_B \\
\mathbf{M}_a &= \frac{\partial^2 T_a}{\partial \dot{\vec{\Theta}}^2} \\
\vec{\tau}_a &= \mathbf{M}_a\ddot{\vec{\Theta}}_a + \vec{\Omega} \times \left[\mathbf{M}_a\dot{\vec{\Theta}}\right] + \dot{\mathbf{M}}_a\dot{\vec{\Theta}}_a - \frac{\partial T_a}{\partial \vec{\Theta}_a},
\end{aligned} \tag{7}$$

where $\dot{\mathbf{M}}_a = 0_{3\times 3}$ and $\dfrac{\partial T_a}{\partial \vec{\Theta}_a} = 0_{3\times 1}$. Equation (7) can then be substituted into (5) to solve for the actuator accelerations that are required to render the inertia, giving

$$\begin{aligned}
\ddot{\vec{\Theta}}_m &= \mathbf{M}_{12}^{-1}\left[\vec{\tau}_a - \mathbf{M}_{11}\ddot{\vec{\Theta}}_a - \vec{\Omega} \times \left[\begin{bmatrix} \mathbf{M}_{11} & \mathbf{M}_{12} \end{bmatrix}\dot{\vec{\Theta}}\right]\right. \\
&\quad \left. - \begin{bmatrix} \dot{\mathbf{M}}_{11} & \dot{\mathbf{M}}_{12} \end{bmatrix}\dot{\vec{\Theta}}\right].
\end{aligned} \tag{8}$$

Inserting (8) into (6) yields the control law.

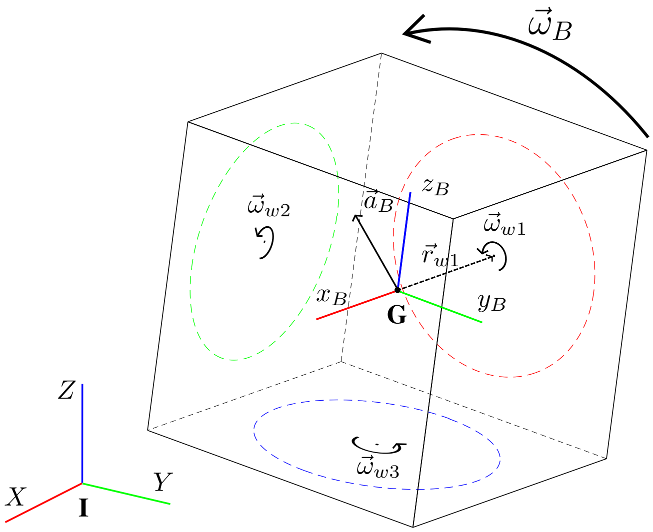

Fig. 2: General layout for an inertia generator using three flywheels.

B. Flywheels Concept

As a basis for comparison, a second model is built using a different method to provide the ungrounded torques. It is based on the GyroCube [10] and the Cubli [11], and comprises three orthogonal flywheels attached to a frame which are independently actuated. This concept, referred to as the flywheels concept, has the advantage of being simple and easy to build, but it lacks efficiency as the flywheels are only free to rotate about a single axis. This means that they act as dead weights when the device is rotated along a different axis.

The process to obtain the dynamics and the control law is similar. Such a concept is illustrated schematically in Figure 2. Firstly, the angular velocities are given by

$$\begin{aligned}
[\vec{\omega}_f]_B &= [\omega_x,\ \omega_y,\ \omega_z]^{\mathrm{T}} \\
[\vec{\omega}_{w1}]_B &= \dot{\phi}\vec{e}_1 + [\vec{\omega}_f]_B \\
[\vec{\omega}_{w2}]_B &= \dot{\theta}\vec{e}_2 + [\vec{\omega}_f]_B \\
[\vec{\omega}_{w3}]_B &= \dot{\psi}\vec{e}_3 + [\vec{\omega}_f]_B \,,
\end{aligned}$$

and the velocities of the centre of mass of the flywheels are given by

$$[\vec{v}_{wi}]_B = [\vec{\omega}_f]_B \times [\vec{r}_{wi}]_B \,.$$

where $\vec{r}_{wi}$ is the position vector of the centre of mass of flywheel $i \in \{1,2,3\}$. Thus, the kinetic energies are given by

$$\begin{aligned}
T_f &= \frac{1}{2}\,[\vec{\omega}_f]_B^{\mathrm{T}}\,[\mathbf{I}_f]_B\,[\vec{\omega}_f]_B \\
T_{wi} &= \frac{1}{2}m_{wi}\,[\vec{v}_{wi}]_B^{T}\,[\vec{v}_{wi}]_B + \frac{1}{2}\,[\vec{\omega}_{wi}]_B^{\mathrm{T}}\,[\mathbf{I}_{wi}]_B\,[\vec{\omega}_{wi}]_B \,,
\end{aligned}$$

where m_{wi} is the mass of flywheel i. As gravity is neglected no potential energy terms are added. Equations (1)-(8) are then applied identically.

III. Model Simulation and Validation

To test the feasibility and performance of each type of 3-DOF rotational inertia generator, simulations were performed using both *Simulink* and *Adams View*. *Simulink* was used to implement a mathematical model of the system, while *Adams View* acted as a form of validation through a physical model simulation. It is to be noted that all simulations neglect gravity because such a device would be designed to ensure that the centre of mass is stationary during its use. This constraint keeps the device from having to provide a constant torque while in use. Friction forces are also neglected.

The simulations were conducted using physical parameters somewhat based on the Cubli [11], in order to obtain realistic data which could help designing a prototype. As such, both simulated objects are composed of an aluminium frame corresponding to a 15 cm-sided box with six walls of 2 mm thickness. This gives the frame a total mass of 0.271 kg and an inertia along its centre of mass of $1.882 \times 10^{-3}\ \mathrm{kg\,m^2}$ in each of the three Cartesian axes. The flywheels design has six thin rings attached to each of the walls, with a mass of 0.102 kg, and an inertia of $0.285 \times 10^{-3}\ \mathrm{kg\,m^2}$ about their rotation axis and $0.143 \times 10^{-3}\ \mathrm{kg\,m^2}$ about perpendicular axes. This arrangement differs slightly from what is shown in Figure 2, but it yields a design in which the geometrical centre and the centre of mass coincide. The original three flywheels are split up into pairs attached to opposite walls. To keep the models comparable, the inertia of both objects need to be kept similar. Mass, on the other hand, can be cut down because it has no influence on the DGG concept. As such, the DGG has a flywheel with a mass of 0.204 kg, and the inertia is set at $0.570 \times 10^{-3}\ \mathrm{kg\,m^2}$, the same as two flywheels, so that the devices will require identical torques to accelerate their rotating parts in a single-axis scenario. This means that the masses and inertias of the gimbals from Figure 1 are neglected. Finally, the prescribed inertia is defined as being that of a solid cube of identical size and with twice the mass of the devices, distributed uniformly, so that $\mathbf{I}_a = 6.62 \times 10^{-3}\ \mathrm{kg\,m^2}$ for each of the three axes.

Using the above physical parameters, a simulation scenario is established. The device is rotated about an arbitrary axis set in the $[2,\ 1, -2]^{\mathrm{T}}$ direction. The angular trajectory about that axis is set as

$$\theta(t) = \theta_A \sin(2\pi f t), \tag{9}$$

where $\theta_A = 60°$ and $f = 0.4$ Hz. An initial velocity of 500 RPM is also added to all six wheels in order to avoid the higher friction zone when a motor operates near or crosses 0 RPM. For the DGG, the single flywheel is also set at 500 RPM, with its initial position parallel to the top and bottom of the frame. In *Simulink*, these inputs are used to compute (8), which allows to compute the resulting moments on the frame (5). This data set is used as a comparison basis using *Adams*, where the computed accelerations are used as inputs to verify if the resulting moments are identical. Figure 3 shows the rendered moments from both simulations in *Simulink* and *Adams*. As it can be observed, the results

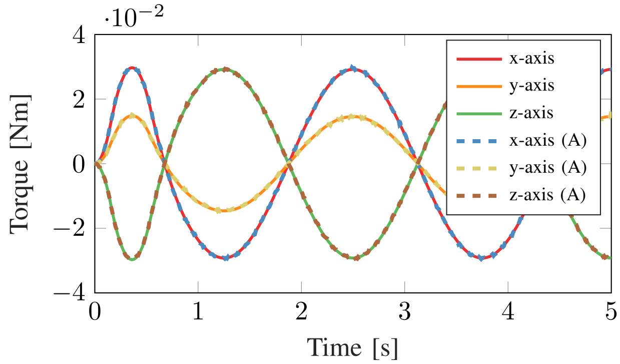

Fig. 3: Simulation results of the $[2,\ 1, -2]^{\mathrm{T}}$ axis of rotation for each of the concepts. Dashed lines represent *Adams* results. The results are identical and cannot be distinguished.

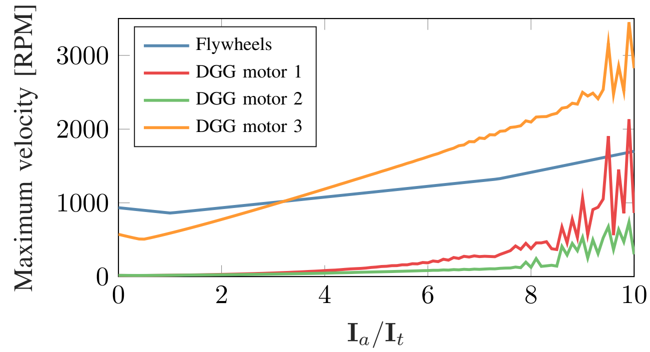

(a) Maximum output angular velocity

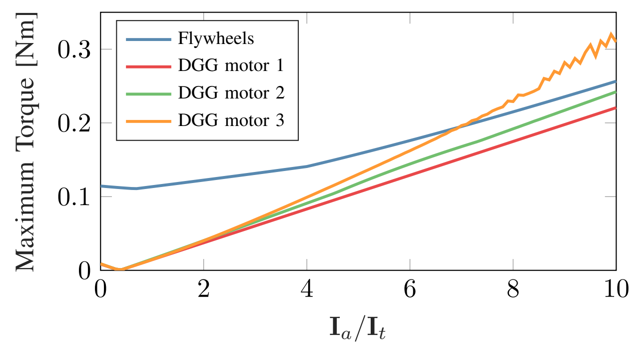

(b) Maximum output torque

Fig. 4: Simulation results for the motor requirements with respect to the rendered inertia for both models.

show that the control laws developed in Section II can theoretically accomplish the established task. It induces the necessary torques on a user so that the device feels like one with the prescribed inertia.

While this is a promising result, more information is needed to determine if the concepts are feasible. Since motors have torque and velocity limits, it is necessary to examine whether the requirements for this type of work are realistic. To do so, simulations are conducted using the parameters mentioned above, while gradually increasing the virtual inertia of the device. As a reference basis, the total inertia from the flywheels concept is used, which is to say that $\mathbf{I}_t = 5.11 \times 10^{-3}\ \mathrm{kg\,m^2}$ for each of the axes. Inertia is varied from $\mathbf{I}_a = 0\ \mathbf{I}_t$ to $\mathbf{I}_a = 10\ \mathbf{I}_t$. The results are shown in Figure 4. For the flywheels concept, only the overall maxima are taken into account for each result as this concept requires symmetry, meaning all three motors need to be identical. For the DGG concept, some simulation instability appears for results where $\mathbf{I}_a > 8\ \mathbf{I}_t$. This could be due to step size and integration method issues, which become critical if the device comes close to a singular configuration where the innermost gimbal is at an angle of 90° from the initial configuration shown in Figure 5. The results show that the DGG concept has a key advantage. For the motors controlling the gimbals (motors 1 and 2), the torque requirements are lower than for the flywheels concept, while needing much smaller velocities. This means that it would be possible to use smaller motors paired with gearboxes to achieve the desired behaviour. As this is a hand-held device, total weight is an important consideration to avoid user fatigue from prolonged use. Motors can make up a considerable portion of the total weight, therefore this is a favourable characteristic to look for. The third motor, the one driving the flywheel, requires more demanding specifications than for the flywheels concept. This entails using a more massive motor, which can be used to the advantage of the concept. Because this motor is located close to the centre of the device, it provides usable inertia when rotating the device about the X and Y-axes. For the flywheels concept, this does not hold true as the motors are directly attached to the frame. As such, they act as dead weights when they are not in use. Overall, this makes the DGG concept a much more interesting design dynamics-wise. It also yields a lighter device (0.408 kg lighter than the flywheels concept). Nevertheless, challenges arise when taking wiring and actuation into account.

IV. Prototyping

A. Mechatronic Configuration

The observations made in the previous section led to choosing the DGG concept for a prototype. A CAD model and a photograph of the prototype are shown in Figure 5. The frame, the gimbals, and the support of the flywheels are made of 3D-printed ABS plastic. The shafts and the links between the motors and the flywheels are made of aluminium, and the flywheels themselves are made of stainless steel. This maximizes the inertia that they provide per volume. The flywheels have been split into two identical annuli in order to place a gimbal motor at the centre, ensuring that the centre of mass is stationary when the device is operated. An additional motor was added for design convenience and therefore the two flywheels can be controlled independently if desired. This gives the device a total mass of 1.392 kg, and it measures 23.85 cm long, 22.2 cm wide and 14.4 cm high. When including the handles, the force/torque sensors and the support legs, it is 45 cm long and 18.2 cm high.

The first two motors are 11 W Re-Max 24 with brushes, from Maxon Motor, paired with 29:1 GP22C planetary gear-

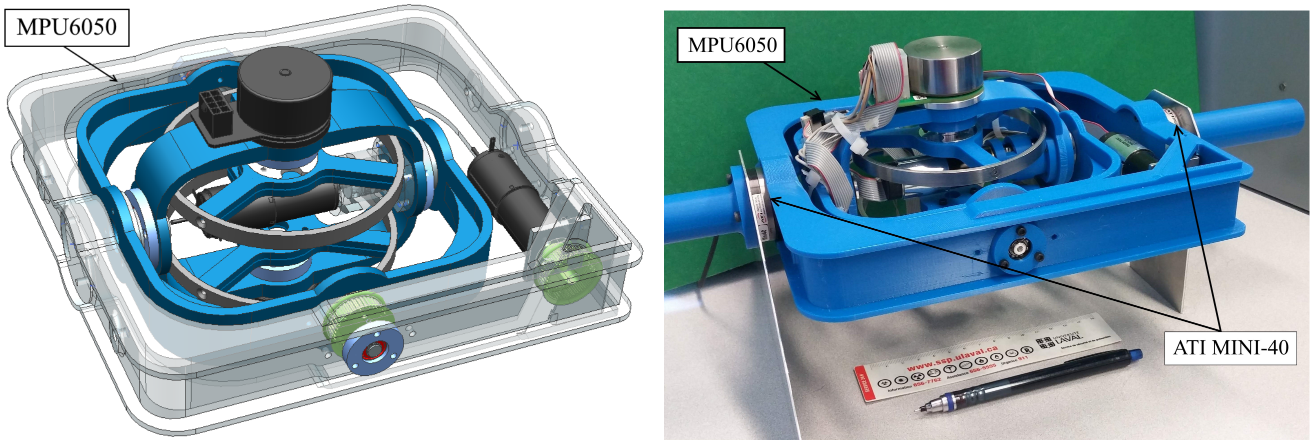

Fig. 5: CAD model and photograph of a prototype of an inertia generator using a double gimbal gyroscope as a means of providing ungrounded torque feedback.

heads. The flywheel motors are 70 W EC-45 Flat brushless DC motors, also from Maxon Motor, used in direct drive. The motors are powered by an external current source which is connected to a computer running the real-time operating system QNX, which ensures real-time computations through *RT-Lab*. An MPU6050 6-DOF IMU is placed on the frame to measure the angular velocity of the frame. It connects to an Arduino Uno through the I2C protocol to read the data. The Arduino sends the data to the real-time computer using its serial interface, with a MAX3232 board to convert the serial pins to RS232 interface. On the software side, *RT-Lab* is used, which compiles *Simulink* models on the real-time computer for the control of the hardware. Figure 6 shows a diagram of the electronic configuration.

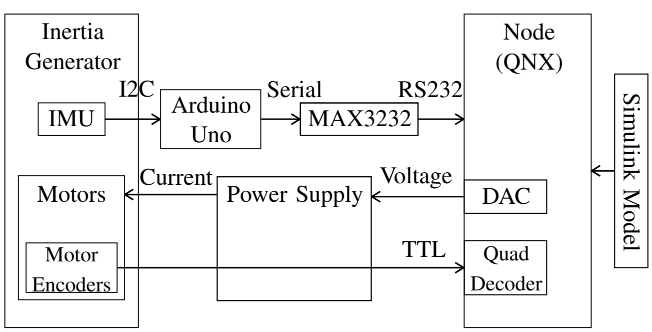

Fig. 6: Communication and electrical layout for the control of the inertia generator.

B. Dynamic Modelling

Since the centres of mass of the components of the prototype do not all coincide perfectly with the global centre of mass, modifications are made to the dynamic model. Any extra component is treated as being part of either the frame or the gimbals. Regarding the motors, the first one is incorporated into the physical properties of the frame, while the other three motors are combined with the innermost gimbal. Thus, while angular velocities are the same as in Section II-A, additional terms need to be included in the model to account for the displacements of the centre of mass of the different bodies. The corresponding velocities of the centres of mass are written as

$$\begin{aligned}
[\vec{v}_f]_B &= \frac{\mathrm{d}}{\mathrm{dt}}[\vec{r}_f]_B + [\vec{\omega}_f]_B \times [\vec{r}_f]_B \\
[\vec{v}_{g1}]_1 &= \frac{\mathrm{d}}{\mathrm{dt}}[\vec{r}_{g1}]_1 + [\vec{\omega}_{g1}]_1 \times [\vec{r}_{g1}]_1 \\
[\vec{v}_{g2}]_2 &= \frac{\mathrm{d}}{\mathrm{dt}}[\vec{r}_{g2}]_2 + [\vec{\omega}_{g2}]_2 \times [\vec{r}_{g2}]_2 \\
[\vec{v}_w]_2 &= \frac{\mathrm{d}}{\mathrm{dt}}[\vec{r}_w]_2 + [\vec{\omega}_{g2}]_2 \times [\vec{r}_w]_2 \,,
\end{aligned}$$

with $\vec{r}_i$ being the position of the centre of mass of body i with respect to the overall centre of mass, which is the reference for the inertial frame. The kinetic energies are thus given by

$$\begin{aligned}
T_f &= \frac{1}{2}m_f [\vec{v}_f]_B^{\mathrm{T}} [\vec{v}_f]_B + \frac{1}{2}[\vec{\omega}_f]_B^{\mathrm{T}} [\mathbf{I}_f]_B [\vec{\omega}_f]_B \\
T_{g1} &= \frac{1}{2}m_{g1} [\vec{v}_{g1}]_1^{\mathrm{T}} [\vec{v}_{g1}]_1 + \frac{1}{2}[\vec{\omega}_{g1}]_1^{\mathrm{T}} [\mathbf{I}_{g1}]_1 [\vec{\omega}_{g1}]_1 \\
T_{g2} &= \frac{1}{2}m_{g2} [\vec{v}_{g2}]_2^{\mathrm{T}} [\vec{v}_{g2}]_2 + \frac{1}{2}[\vec{\omega}_{g2}]_2^{\mathrm{T}} [\mathbf{I}_{g2}]_2 [\vec{\omega}_{g2}]_2 \\
T_w &= \frac{1}{2}m_w [\vec{v}_w]_2^{\mathrm{T}} [\vec{v}_w]_2 + \frac{1}{2}[\vec{\omega}_w]_2^{\mathrm{T}} [\mathbf{I}_w]_2 [\vec{\omega}_w]_2 \,.
\end{aligned}$$

C. Experimental Validation

By using the full control law, experiments are conducted to validate the model developed in Section II. To achieve this, a comparison is made between the moments calculated with (5), and the real moments applied to the prototype. First, two ATI MINI-40 force/torque sensors are mounted on each side of the frame, with handles attached so that all torques rendered to the user are measured by the sensors. This arrangement can be seen on the photograph shown in Figure 5. Then, an arbitrary rotational trajectory is applied to the device by a user. Lastly, the moments measured by the force/torque sensors are compared to those computed by (5), using the measurements provided by the MPU6050 and the motor encoders. To have a diversity of results, four experiments are performed. The first is meant as a validation of expected behaviour by simulating the total inertia $\mathbf{I}_t$ of

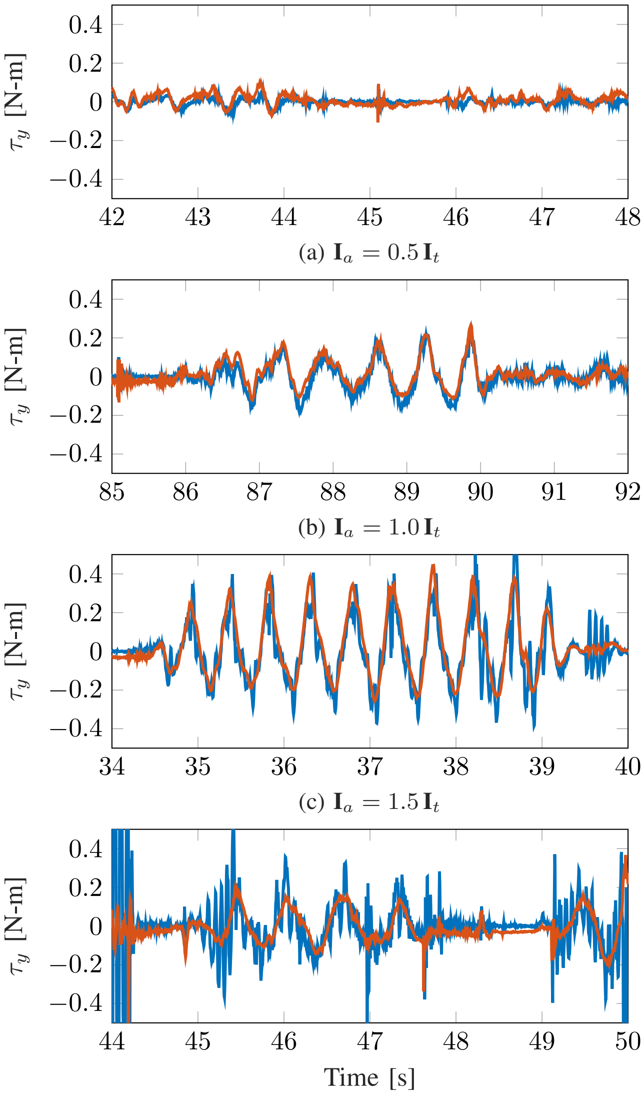

(a) $\mathbf{I}_a = 0.5\,\mathbf{I}_t$

(b) $\mathbf{I}_a = 1.0\,\mathbf{I}_t$

(c) $\mathbf{I}_a = 1.5\,\mathbf{I}_t$

(d) $\mathbf{I}_a = 2.5\,\mathbf{I}_t$

Fig. 7: Comparison of the torques applied to the frame by the user for a variety of simulated inertias. Flywheels are initially at rest. Measurements in red come from force/torque sensors, and the blue curve is computed using the dynamic model. Device trajectories were similar except for $2.5\,\mathbf{I}_t$ where instabilities prevented large amplitude movements.

the device. The others explore the capabilities of the inertia generating functions by setting the simulated inertia at 0.5, 1.5 and 2.5 $\mathbf{I}_t$ respectively.

For the first experiment, the simulated inertia is set at $\mathbf{I}_a = \mathbf{I}_t$, with both flywheels starting at an initial velocity of 0 RPM. The device is then picked up and moved in various directions. With these parameters, it is expected that the gimbals would stay in place, making the whole device move as a rigid body. The moments applied to the frame by the user to induce movement are shown in Figure 7 (b). As it can be seen, the dynamic model produces results that are close to the measured torques. Some noise is present in both data sets, since force sensors are noisy, and the model data uses angular velocities and accelerations derived from the motor encoders. This agreement between both data sets confirms that the dynamic model is accurate.

The other experiments are conducted using a similar procedure, with the only difference that the simulated inertia is set at 0.5, 1.5, and 2.5 $\mathbf{I}_t$ respectively. The initial velocity of the flywheels is kept at 0 RPM even though it was meant to be used at high velocities. This is due to instability issues which are discussed in Section V. Due to the repetitive nature of the results, only the Y-axis data from each experiment is shown in Figure 7. As with the previous experiment, the force/torque sensor data concurs with the dynamic model in the first two sets of data. When simulated inertia is set too far from the device's total inertia, some vibration occurs in the motors which can be seen in the dynamic model data of Figure 7 (d) because it uses the motor encoder data. The force/torque sensors did not fully pick up these vibrations, even though they could be felt and heard by the user. Their nature is currently thought to be linked with the PID tuning of the motor position controls. Vibrations notwithstanding, the sensor data follows the general pattern of the model data.

V. Discussion

At first glance, the results presented above are encouraging, yielding evidence that inertia rendering is a feasible concept. Indeed, Figures 7 (a) and 7 (c) show that increasing the virtual inertia of the device does require more torque from the user's part. The increase appears more substantial than it actually is. The difference is attributed to the arbitrary nature of the trajectories imposed by the user. Indeed, the gyro data associated with Figure 7 (c), which is not presented, shows that the amplitude of the movement was larger than in Figure 7 (a).

Unfortunately, the above experiments do not make full use of the developed DGG concept. Indeed, it is intended to set the flywheels at a large initial velocity of at least 2000 RPM. In theory, using such velocities helps stabilize the gyroscope because it reduces the required angular range of the gimbals. The faster the flywheels spin, the less the gimbals need to move to produce large gyroscopic effects. In practice, the device reaches instability rather quickly. It is currently thought that this is due to the need to react to an IMU's signal, along with the noise from the IMU and imprecise user movements.

Nonetheless, the experiments conducted in this article are relevant for the development of the concept of inertia generator. The architecture of the DGG prototype is akin to having the flywheels concepts where a single flywheel is mounted in a serial configuration instead of three flywheels mounted in parallel like shown in Figure 2. The introduction of singularities and angular position limitations is detrimental, but the essence remains.

In the present form of the device, cable management is a prominent issue. During the design phase, the idea of hollow shafts was put forth to allow the cables to connect to the motors without hindering the motion of the gimbals. It was also meant to allow the outermost gimbal to make a few revolutions about its axis of rotation. Unfortunately, given the size and number of cables, space limitations did not allow to implement this approach. This issue could be fully circumvented by the use of slip rings, enabling the transmission of power without the risk of twisting the cables during use.

Moreover, because the cables are now attached to the frames without going through the axes of rotation, the gimbals are limited in their range of motion. The 1-DOF prototype [9] also had this type of limitation due to its translational nature. Similar strategies of handling limited displacement are to be implemented. It should be pointed out that the flywheels concept presented in section II-B would have similar issues. While not constrained in terms of angular position, the maximum velocity of the motors is a constraint that yields similar limitations. Some form of washout filter is thus needed to prevent the saturation of the motors.

Lastly, because a gyroscope is an unstable mechanism, divergences happen through the numerical integration of (8). This makes it difficult to use the device for more than a few seconds, even when using a Runge-Kutta method of the 10^{th} order for integration. When used solely as a torque generation method, a gyroscope can function appropriately, but since the inertia generator requires reaction through an IMU which provides noisy data, its unstable nature becomes inadequate. All of the above difficulties were unfortunately harder to account for before completing a working prototype.

An additional step is taken to look back at the simulations conducted in section III. For the comparison between the DGG and the flywheel concept, the working hypothesis was that the gimbals of the DGG could be neglected, both in terms of mass and inertia. In practice, taking data from the prototype, the gimbals weigh 0.199 kg and 0.124 kg respectively, whereas the central flywheels weigh 0.189 kg combined. At first glance, this invalidates the hypothesis, but it is also necessary to take into account that these gimbals add inertia which can be used for torque production, albeit not in all axes. Including the gimbals would have made it difficult to find a valid basis of comparison between both concepts. All in all, the flywheel's inertia is not as prominent as desired when compared to the rest of the system, and thus could be further increased in a future iteration.

VI. Video

The video accompanying this paper demonstrates the strategy used to validate the dynamic model. It uses predetermined trajectories for the gimbals, which are periodic movements, along with a constant velocity for the flywheels. The outermost gimbal performs a sinusoidal trajectory with an amplitude of 50° and a frequency of 1 Hz while the innermost gimbal performs the same type of trajectory with an amplitude of 35° and a frequency of 0.7 Hz. The flywheels rotate at a constant velocity of 750 RPM. The device is then picked up and rotated around the Z-axis, X-axis, and Y-axis. It is finally rotated in one last arbitrary direction before being put back down. The force/torque sensor data and the data computed using the dynamic model are shown in real time, along with the device's angular velocity as measured by the MPU6050.

VII. Conclusion

In this paper, the development of a prototype of a 3-DOF haptic interface with programmable rotational inertia was presented. Simulations of simplified models indicate that there is a significant potential for the feasibility and the performances of a device exploiting the gyroscopic effect.

Experiments using the current prototype suggest that although the DGG is an efficient theoretical concept, it comes with implementation difficulties which prevent it from making use of that efficiency. Nevertheless, its limited functions are sufficient to demonstrate that the 3-DOF inertia generator concept is valid.

Future work will focus on optimizing the control of the device and managing the angular position limitations of the gimbals. A form of washout filter will be needed to achieve this. Moreover, comparing the DGG to a flywheels prototype is planned in order to quantify the advantages of better stability and full range of angular motion. Finally, this work is to be extended to the development of a 6-DOF inertia generator, which would combine rotational and translational inertia control.

References

[1] J.-P. Choiniere and C. Gosselin, "Development and experimental validation of a haptic compass based on asymmetric torque stimuli," *IEEE Transactions on haptics*, vol. 10, no. 1, pp. 29–39, 2016.

[2] W. Heuten, N. Henze, S. Boll, and M. Pielot, "Tactile wayfinder: a non-visual support system for wayfinding," in *Proceedings of the 5th Nordic conference on Human-computer interaction: building bridges*, 2008, pp. 172–181.

[3] H. Yano, M. Yoshie, and H. Iwata, "Development of a non-grounded haptic interface using the gyro effect," in *11th Symposium on Haptic Interfaces for Virtual Environment and Teleoperator Systems*. IEEE, 2003, pp. 32–39.

[4] S. Heo, C. Chung, G. Lee, and D. Wigdor, "Thor's hammer: An ungrounded force feedback device utilizing propeller-induced propulsive force," in *Proceedings of the 2018 CHI Conference on Human Factors in Computing Systems*, 2018, pp. 1–11.

[5] J. Gugenheimer, D. Wolf, E. R. Eiriksson, P. Maes, and E. Rukzio, "Gyrovr: Simulating inertia in virtual reality using head worn flywheels," in *Proceedings of the 29th Annual Symposium on User Interface Software and Technology*, 2016, pp. 227–232.

[6] P. Ramsamy, A. Haffegee, R. Jamieson, and V. Alexandrov, "Using haptics to improve immersion in virtual environments," in *International Conference on Computational Science*. Springer, 2006, pp. 603–609.

[7] K. N. Winfree, J. Gewirtz, T. Mather, J. Fiene, and K. J. Kuchenbecker, "A high fidelity ungrounded torque feedback device: The itorqu 2.0," in *World Haptics 2009*. IEEE, 2009, pp. 261–266.

[8] C. Swindells, A. Unden, and T. Sang, "Torquebar: an ungrounded haptic feedback device," in *Proceedings of the 5th international conference on Multimodal interfaces*, 2003, pp. 52–59.

[9] C. Gosselin, A. Lecours, T. Laliberté, and M. Fortin, "Design and experimental validation of planar programmable inertia generators," *The International Journal of Robotics Research*, vol. 33, no. 4, pp. 489–506, 2014.

[10] M. Sakai, Y. Fukui, and N. Nakamura, "Effective output patterns for torque display'gyrocube'," in *Online Proceeding of the 13th International Conference on Artificial Reality and Telexistence, December 3-5, 2003*, 2003.

[11] M. Gajamohan, M. Merz, I. Thommen, and R. D'Andrea, "The cubli: A cube that can jump up and balance," in *2012 IEEE/RSJ International Conference on Intelligent Robots and Systems*. IEEE, 2012, pp. 3722–3727.